aerospace

MDPI

Article

Numerical Investigation of Transverse-Jet-Assisted Initiation of Oblique Detonation Waves in a Combustor

Zijian Zhang * and Ziqi Jiang

Department of Aeronautical and Aviation Engineering, The Hong Kong Polytechnic University, Hong Kong, China
* Correspondence: zijzhang@polyu.edu.hk

Abstract: Detonation initiation is a prerequisite to normal operations of an oblique detonation engine (ODE), and initiation-assistant measures are imperative in cases of initiation failure that occur in a length-limited combustor under wide-range flight conditions. This study numerically investigates the initiation characteristics of oblique detonation waves (ODWs) in H_2-fueled ODE combustors at wide-range flight Mach numbers Ma_f or flight altitudes H_f. Failures of ODW initiation are observed at both low Ma_f and high H_f if no measure is taken to assist initiation. Through analyses of the flow fields and theoretical predictions of the ignition induction length L_{ind}, the data reveal that the detonation failure at low Ma_f is raised by the significant decrease in the post-shock temperature due to insufficient shock compression, leading to a significant increase in L_{ind}. The detonation failure at high H_f is caused by the rapid decrease in the combustor inflow pressure as H_f increases, which also results in an increase in L_{ind}. With further identifications of the key flow structures crucial to detonation initiation, an initiation-assistant concept employing a transverse H_2 jet is proposed. The simulation results show that through an interaction between the incident oblique shock wave and the jet shock wave, the transverse jet helps to initiate an ODW in the combustor at a low Ma_f, and the initiation location is relatively fixed and determined by the jet location. At high H_f, a Mach reflection pattern is formed in the combustor under the effects of the transverse jet, and detonative combustion is achieved by the generated Mach stem and its reflected shock waves. The proposed concept of using transverse jets to assist detonation initiation provides a practical reference for future development of ODEs that are expected to operate under wide-range flight conditions.

Keywords: oblique detonation wave; initiation; transverse jet; oblique detonation engine; wide-range flight condition

Citation: Zhang, Z.; Jiang, Z. Numerical Investigation of Transverse-Jet-Assisted Initiation of Oblique Detonation Waves in a Combustor. *Aerospace* **2023**, *10*, 1033. https://doi.org/10.3390/aerospace10121033

Academic Editors: James 'Chris' Thomas and Sergey Leonov

Received: 27 October 2023
Revised: 12 December 2023
Accepted: 13 December 2023
Published: 14 December 2023

1. Introduction

Driven by the motivation to achieve faster and more efficient atmospheric transportation, the research into and development of hypersonic aircraft have rapidly increased in recent decades [1,2], and the relevant propulsion system has become a technical bottleneck limiting further advancements [3,4]. By forming a stabilized oblique detonation wave (ODW) in the combustor to replace the traditional diffusive combustion mode, an oblique detonation engine (ODE) is a promising propulsion solution for future hypersonic flights [5,6]. As one type of extreme combustion phenomenon featuring tight coupling between a shock wave and a flame, detonation is capable of providing high efficiency in chemical-to-mechanical energy conversion and consequently increasing the propulsion performance [7,8]. The rapid heat release rate of the detonative combustion mode also implies a short combustor, which helps to reduce the massive heat losses and frictions on walls, simplify the thermal management system, and reduce the total weight of the engine [9,10]. Moreover, an ODW is expected to self-adapt to various flow perturbations by adjusting its wave angle, which benefits the stable operation of the ODE. Recently, such an oblique detonation propulsion solution using gaseous hydrogen or liquid aviation kerosene as the fuel has been experimentally demonstrated in a hypersonic shock tunnel [11,12], which signifies that ODEs are anticipated to be used in the near future. However, various technical difficulties associated with ODEs, such as hypersonic mixing, premature ignition prevention, oblique detonation initiation, and stabilization, still need to be fully solved before ODEs can be implemented in practical applications.

An ODW is typically formed when a high-speed combustible mixture flows through a wedge [13]. A numerical study conducted by Li et al. [14] showed that a wedge-induced ODW generally transitions from a nonreactive oblique shock wave (OSW), which was later supported by the experimental observations obtained by Viguier et al. [15] and Lin et al. [16]. Further simulations found that the detailed OSW–ODW transition patterns can be classified into two main types: smooth with a curved shock front and abrupt with a multiwave point [17,18]. More complex flow structures within the induction zone of an ODW under certain flow conditions have been reported by Liu et al. [19] and Yang et al. [20]. In engineering applications, the wedge length needed for ODW initiation (i.e., the transition length from an OSW to an ODW) is more important and shows great sensitivities to the free-stream parameters [21], mixture reactivity [22], and wedge angle [23].

An ODE is commonly designed at one single point, whereas in practical applications, the system operates under a wide range of flight Mach numbers and flight altitudes. Under off-design conditions (for example, at low flight Mach numbers), the initiation length of ODW could be significantly increased due to the insufficient compression of the OSW [22,24]. When the ODW initiation length is much longer than the length scale of the ODE combustor, detonation initiation failure occurs, and consequently, the engine might be unable to generate thrust [25–27]. A similar detonation initiation issue could emerge when the ODE is operated at high altitudes where the atmospheric temperature does not change much but the pressure drops drastically [24,28]. Therefore, detonation initiation within a length-limited combustor under wide-range flight conditions needs to be further examined and investigated to advance the implementation of ODEs in practical applications.

Many novel methods or concepts have been proposed to control and promote ODW initiation. The direct initiation of ODWs by spherical blunt bodies has been widely studied through high-speed projectile-launching experiments, and the criticalities of the formation of stabilized ODWs have been discussed [29,30]. Fang et al. [31] numerically investigated the direct initiation of ODWs induced by blunted wedges, and a theoretical criterion based on the detonation cell sizes was proposed to predict the critical blunt radius. The effectiveness of leading-edge blunting in the initiation assistance of wedge-induced ODWs was experimentally validated by Gong et al. [32]. Other modifications to a pure wedge geometry to facilitate the rapid initiation of ODWs include the use of a step [33], dual-angle wedges [34,35], curved wedges [36,37], etc. Inspired by the formation mechanism of the abrupt OSW–ODW transition pattern, Han et al. [38] proposed introducing a small bump on the wedge surface to promote ODW initiation through shock/shock interactions. The effectiveness of such a concept was later validated numerically by Xiang et al. [39] and experimentally by Han et al. [12].

Hot jets have been widely employed in detonation-based engines [40,41]. Han et al. [42] discussed, in terms of the relationship between the inflow velocity and the detonation velocity, the formations and propagations of two types of detonations that are triggered by hot jets in supersonic premixed flows. The formation process of a detonation wave initiated by a hot transverse jet was numerically investigated by Cai et al. [43,44], and the role of a contracting flow channel formed by the hot jet on the propagation of the detonation wave was analyzed. The initiation characteristics of ODWs via a combination of a jet and a wedge were studied numerically by Yao & Lin [45], and the transformations of different combustion regimes controlled by two nondimensional parameters (i.e., the momentum flux ratio and the penetration ratio) were thus revealed.

In this study, transverse jets are utilized to control initiations of ODWs in two typical ODE combustors designed for wide-range applications of flight Mach number or flight altitude and are numerically investigated. First, the general geometry of a representative

ODE combustor, the mathematical models, the numerical algorithms, and a case summary are introduced in Section 2. Then, the initiation characteristics of ODWs in the combustors without any assistance measures are analyzed for operations in a wide range of flight Mach numbers or flight altitudes in Section 3. This section also includes a thorough discussion of the crucial flow structures for detonation initiation. In Sections 4.1 and 4.2, respectively, the initiation-assistant methods using a transverse jet as well as the corresponding numerical validations for addressing the initiation failure issues at low flight Mach numbers or high flight altitudes are presented. Finally, conclusions are provided in Section 5.

2. Details of the Methodology

2.1. Geometry of an ODE Combustor

This study considers a classical two-dimensional (2-D) configuration of ODEs with external fuel injection [9], as schematically shown in Figure 1a. The inlet is two-stage and is designed to compress the incoming airflow and implement fuel/air mixing. Immediately after the inlet but before the nozzle, there is a short detonative combustor in between, with its detailed geometry illustrated in Figure 1b. The combustor enveloped within points OCDE has a flow channel of a constant height (denoted as DE = h_c). An ODW is generated from the leading edge of the cowl wall (i.e., point C), extends downstream, and reflects over the wall on the other side. According to Zhang et al. [46], the formed ODW is easily destabilized if it is reflected before the first expansion corner of the combustor (i.e., point O); hence, it is suggested to set the reflection locus right at or downstream of the first expansion corner for more redundancy of stabilization. The actual reflection location is determined by the initiation length of the ODW, the wave angle of the ODW, the height of the combustor $h_{c'}$ and the upstream-extending distance of the cowl's leading edge compared to the first expansion corner (denoted as CK = d_c). Notably, the initiation length and the wave angle of the ODW depend on the free-stream parameters. Therefore, it is practical to control the reflection location of the ODW by determining d_c with a fixed h_c based on the most upstream posture of the ODW under the given operation condition range of the ODE, i.e., an ODW with a near-zero initiation length and a maximum wave angle (as shown by the red solid line in Figure 1b).

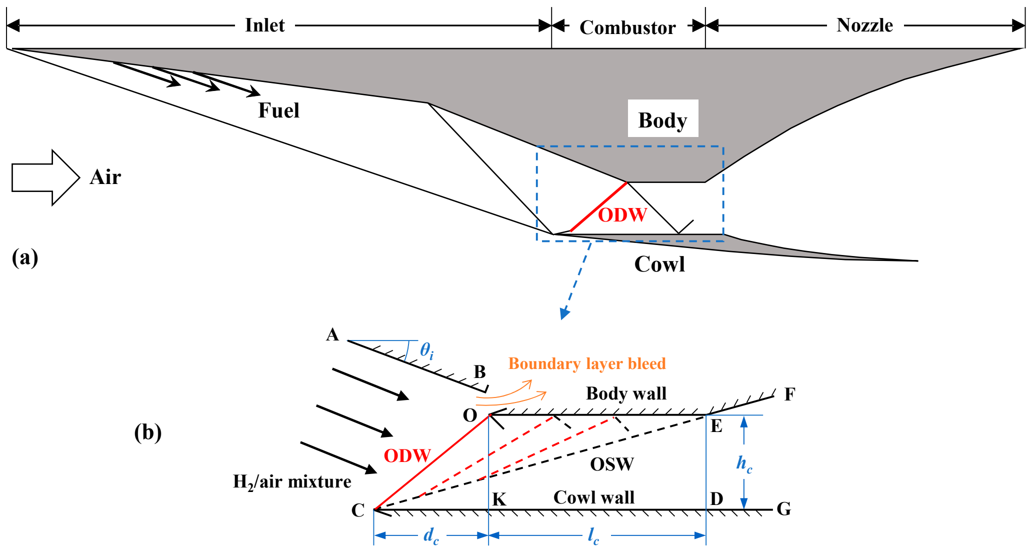

Figure 1. Schematics of (**a**) the classical configuration of an external-injected ODE and (**b**) the detailed geometry of the combustor.

Although the combustor channel has no significant effect on the performance of the ODW (assuming it can be successfully initiated), a considerable length (denoted as OE = l_c) is commonly required to prevent the significant expansion effects of the nozzle on the strength of the OSW and subsequently the initiation of the ODW. Notably, d_c is nearly proportional to h_c for given conditions. Typical and fixed values of h_c = 6 cm and l_c = 20 cm are used in this study, equal to those values employed by Zhang et al. [47]. Then, the value of d_c is determined by the certain operation conditions of the ODE and fixed for the combustor. Upstream of the combustor, the inlet wall has an inclined angle of θ_i, indicating that the flow deflection angle after flowing into the combustor is θ_i as well. To control the growth and upstream motion of the separation zone formed through the ODW/boundary-layer interaction, a simple floor bleed structure is employed at the entrance of the combustor (i.e., point O), which expels the incoming boundary layer from the inlet and reestablishes a thin boundary layer downstream [11,47,48]. Finally, a one-side expanding nozzle is located downstream of the combustor.

2.2. Mathematical Models and Numerical Algorithms

Since the effectiveness of a transverse jet in assisting oblique detonation initiation is the main focus of this study, complex 3-D effects of the flow field, such as 3-D wave structures and boundary layers over the combustor's side walls, are neglected for simplicity [43–45], which is believed to have limited impact on the conclusions. Hence, the flow field in the ODE combustor is governed by the 2-D multispecies reactive Reynolds-averaged Navier-Stokes (RANS) equations. Menter's shear-stress transport (SST) k-ω turbulence model [49] is used to model the turbulent stresses. The well-known NASA Glenn database [50] is used to model the thermodynamic properties of each species. Hydrogen is used as the fuel, and its combustion is modeled by a modified Jachimowski's reaction model [51] involving 19 reversible elementary reactions among 8 species: H_2, H, O_2, O, OH, HO_2, H_2O_2 and H_2O and with N_2 serving as the bathing species. This detailed chemistry mechanism for H_2/air combustion was proved to well predict the ignition delay time [52] and has been widely used in numerical simulations of unsteady shock-induced combustion phenomena [48,53,54] scramjets [55,56], ODWs [45], and ODEs [48,57]. More details regarding the mathematical modeling are available in Zhang et al. [47].

The governing equations are numerically solved using a quadrilateral-grid-based finite volume method [58], where the spatial discretization is implemented through a second-order total variation diminishing (TVD) scheme [59]. The convective flux on each cell edge is evaluated based on a nonlinear Harten–Lax–van Leer contact (HLLC) approximate Riemann solver together with the use of a minmod limiter to suppress the non-physics oscillations that easily occur in the vicinity of flow discontinuities. An implicit dual time-stepping method is adopted for integration in the time direction in time-dependent simulations. The applicability of the above numerical methods to hypersonic reactive flows, including the combustion flow fields in ODEs, has been well demonstrated in, for example, refs. [37,47,48]. In particular, a preliminary comparison of the oblique detonation flow field in an ODE combustor model between a wind-tunnel experiment and a 2-D numerical simulation using the present methods was made in the supplementary materials of Zhang et al. [47], and a good agreement was obtained.

2.3. Cases

The initiations of ODWs in ODE combustors under two types of wide-range operation conditions, i.e., wide-range flight Mach number Ma_f and wide-range flight altitude H_f, are individually investigated. Two sets of inflow parameters and combustor geometric parameters are employed accordingly. First, a wide operation range of the flight Mach number from Ma_f = 8 to 13 is assumed, while the flight altitude is set at H_f = 30 km. To maintain the structural simplicity of the ODE under such wide-range conditions, all the compression angles of the engine are expected to be fixed, and they are typically designed at high-flight Mach numbers to ensure that the post-compression airflow temperature falls within an appropriate range for normal operations. Thus, a fixed inclined angle of θ_i = 16° is set to the inlet wall for the aforementioned wide-range-Ma_f operation conditions.

The inflow parameters such as temperature T_i, pressure $p_{i'}$ and velocity magnitude V_i before entering the ODE combustor for each flight Mach number are estimated through two shock-compressions of two 8° ramps in the inlet, which are summarized in Table 1. The equivalent ratio of the inflows is then assumed to be unity. Furthermore, d_c is set to 73 mm, and then an ideal ODW at Ma_f = 8 would reflect right downstream of point O. In Table 1, Cases 1–6 represent scenarios without any initiation-assistant measures, while Cases 7–10 represent scenarios employing a transverse jet to assist with detonation initiation. More details regarding the transverse-jet-assisted method are provided in Section 4.1.1.

Table 1. Case setups in investigations under wide-range-Ma_f conditions.

Cases No.	Ma_f	H_f (km)	T_i (K)	p_i (kPa)	V_i (m/s)	θ_i	d_c (mm)	h_c (mm)	$\Delta\phi_{\text{jet}}$	$p_{0,\text{ jet}}$ (kPa)	J
1	13	30	795.4	38.25	3775	16°	73	60	–	–	–
2	12	30	731.0	32.17	3480	16°	73	60	–	–	–
3	11	30	670.0	26.74	3184	16°	73	60	–	–	–
4	10	30	612.4	21.94	2889	16°	73	60	–	–	–
5	9	30	558.5	17.75	2593	16°	73	60	–	–	–
6	8	30	508.2	14.15	2296	16°	73	60	–	–	–
7	11	30	670.0	26.74	3184	16°	73	60	0.05	878.5	0.267
8	10	30	612.4	21.94	2889	16°	73	60	0.05	715.3	0.309
9	9	30	558.5	17.75	2593	16°	73	60	0.05	569.7	0.363
10	8	30	508.2	14.15	2296	16°	73	60	0.075	663.0	0.656

Another batch of simulations considers wide-range-H_f operation conditions. In these conditions, a similar combustor to that presented previously is considered, but with the inclined angle of the inlet wall changed to θ_i = 25°. A flight condition of Ma_f = 9 and H_f = 30 km is set as the baseline case. Assuming that the free-stream airflow is compressed by two 12.5°-ramps in the inlet, the inflow parameters before the combustor for this baseline case are T_{ref} = 855.1 K, p_{ref} = 43.96 kPa and V_{ref} = 2466 m/s. In this ODE combustor, d_c is equal to 50 mm, and the design reflection point of the ODW is located 60 mm downstream of point O. Notably, an increase in the flight altitude would result in a near-exponential decrease in atmospheric pressure, but the variation in atmospheric temperature remains relatively small (typically ranging from 210 K to 290 K). For instance, when the flight altitude increases from 20 km to 40 km, the atmospheric pressure decreases from 5529 Pa to 287 Pa, which is approximately 1/20 of the former, whereas the atmospheric temperature only increases from 217 K to 250 K (by approximately 15%). Similarly, in the case of an ascent from 20 km to 50 km, the atmospheric pressure of the latter altitude even decreases to approximately 1/70 of the former altitude, while the atmospheric temperature increases by approximately 25% from 217 K to 271 K.

Clearly, the major effects of different flight altitudes on ODW initiations come from the near-exponential variation in the combustor's inflow pressure because the pressure and temperature ratios are correlated with each other during the inlet compression process, and the inflow temperature before the combustor should be limited for premature ignition prevention (e.g., below approximately 900 K for hydrogen-fueled ODEs). In this case, we investigate this problem more simply by varying the inflow pressure p_i before the combustor with reference to the baseline case but keeping other flow parameters such as inflow temperature and velocity unchanged (i.e., T_i = T_{ref} and V_i = V_{ref}). Specifically, the inflow pressure in the simulated cases, as summarized in Table 2, decreases from p_i = p_{ref} to 0.2 p_{ref}, 0.1 p_{ref}, 0.05 p_{ref}, and finally, 0.025 p_{ref}. The corresponding flight altitude in terms of atmospheric pressure increases from approximately H_f = 30 km to 41 km, 47 km, 52 km, and finally, 57 km. In Table 2, Cases 11–15 represent scenarios without employing any initiation-assistant measure, whereas Case 16 serves as a control counterpart to Case 15 to validate the effectiveness of using a transverse jet in ODW initiation (as is discussed further in Section 4.2).

Table 2. Case setups in investigations under wide-range-H_f conditions.

Cases No.	Ma_f	H_f (km)	T_i (K)	p_i (kPa)	V_i (m/s)	θ_i	d_c (mm)	h_c (mm)	$\Delta\phi_{\mathrm{jet}}$	$p_{0,\mathrm{jet}}$ (kPa)	J
11	9	30	855.1	43.96	2466	25°	50	60	–	–	–
12	9	41	855.1	8.79	2466	25°	50	60	–	–	–
13	9	47	855.1	4.40	2466	25°	50	60	–	–	–
14	9	52	855.1	2.20	2466	25°	50	60	–	–	–
15	9	57	855.1	1.10	2466	25°	50	60	–	–	–
16	9	57	855.1	1.10	2466	25°	50	60	0.2	42.50	1.73

In all cases, a grid resolution of 0.1 mm × 0.1 mm at maximum is used in the core flow regions. Near the walls, the grids are clustered in the normal direction with a minimum height of 2 μm. This grid resolution setup is similar to that used in the authors' previous study [47] and was proved suitable for capturing the key characteristics of ODW initiation.

3. Initiation Characteristics of ODWs without Assistant Measures

3.1. ODW Initiation Characteristics in the Combustor at Different Ma_f

The flow fields of the combustor at Ma_f = 13, 12, 11, 10, 9, and 8 without employing any initiation-assistant measures (i.e., Cases 1 to 6 in Table 1) are depicted in Figure 2 as the temperature and H_2 mole fraction contours superimposed with pressure isolines. At Ma_f = 13 and 12 (as shown in Figure 2a,b), the rapid combustion of the inflowing H_2/air mixture is induced at the high temperature (>1300 K) behind the OSW formed from the cowl's leading edge, and thus, an ODW is initiated from the OSW at a rather short distance (defined as the OSW–ODW transition length $L_{\mathrm{tran}'}$ as illustrated in Figure 2a,b). On the body side, the ODW reflects downstream of the leading edge of the upper wall of the combustor, which induces the formation of a large-scale separation zone. Overall, the combustion of the inflowing mixture is mainly completed through the ODW in these two high Ma_f cases, resulting in a predominant percentage of the oblique detonative combustion mode in the combustor.

When the flight Mach number decreases to Ma_f = 11 (as shown in Figure 2c), the post-shock temperature of the OSW decreases to a relatively lower value of approximately 1180 K, leading to an apparent increase in the ignition delay time and, subsequently, the OSW–ODW transition length. As a result, the percentage of the oblique detonative combustion mode reduces significantly to approximately 50%, although an ODW is successfully initiated in the combustor at this Ma_f. The remaining fuel of the mixture is burned behind the OSW with a slower combustion rate, which is considered a deflagrative combustion mode.

When the flight Mach number further decreases to Ma_f = 10 (as shown in Figure 2d), the post-shock temperature of the OSW decreases to approximately 1050 K, and the corresponding ignition delay time and the OSW–ODW transition length are so large that the formed OSW fails to directly transition to an ODW within the given combustor length. In this case, a certain percentage of the oblique detonative combustion mode still occurs in the combustor through the reflected shock waves (RfSWs) in the regular interaction between the OSW and the leading-edge separated shock wave (SSW).

At a lower-flight Mach number of Ma_f = 9 (as shown in Figure 2e), the post-OSW temperature is merely approximately 930 K, and similarly, no initiation of an ODW from the OSW occurs. Furthermore, no detonative combustion is induced by possible alternate flow structures in the combustor such as the RfSWs in the case of Ma_f = 10. Only some mild combustion emerges near the walls in the latter part of the combustor, but the mixture flows into the nozzle and undergoes an expansion soon. Obviously, the combustion efficiency in this case is very low, which might be insufficient to generate enough thrust for normal operations. At Ma_f = 8, the lower design limit of the ODE, no combustion is observed in the combustor (as shown in Figure 2f), implying a complete failure of the engine.

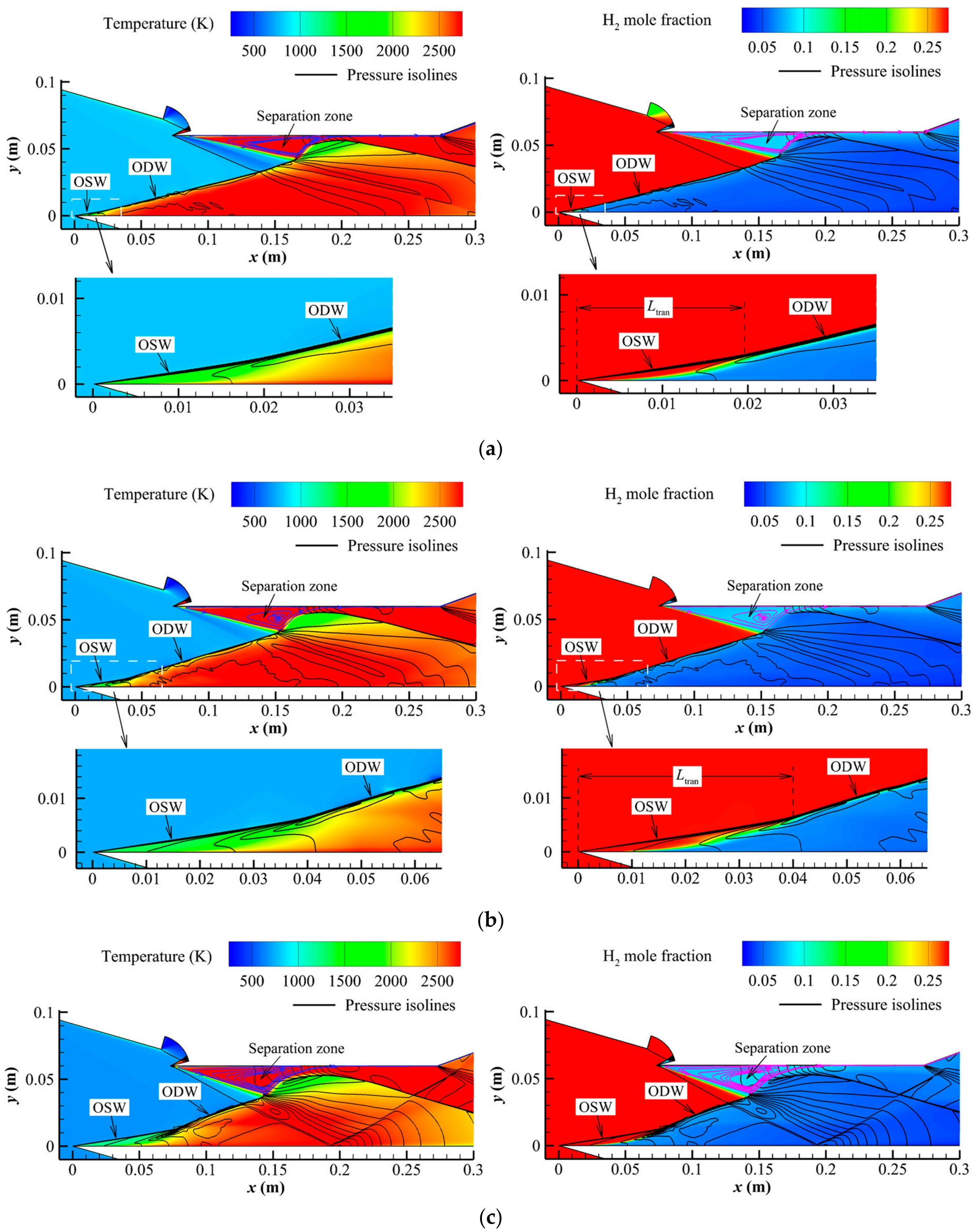

Figure 2. *Cont*.

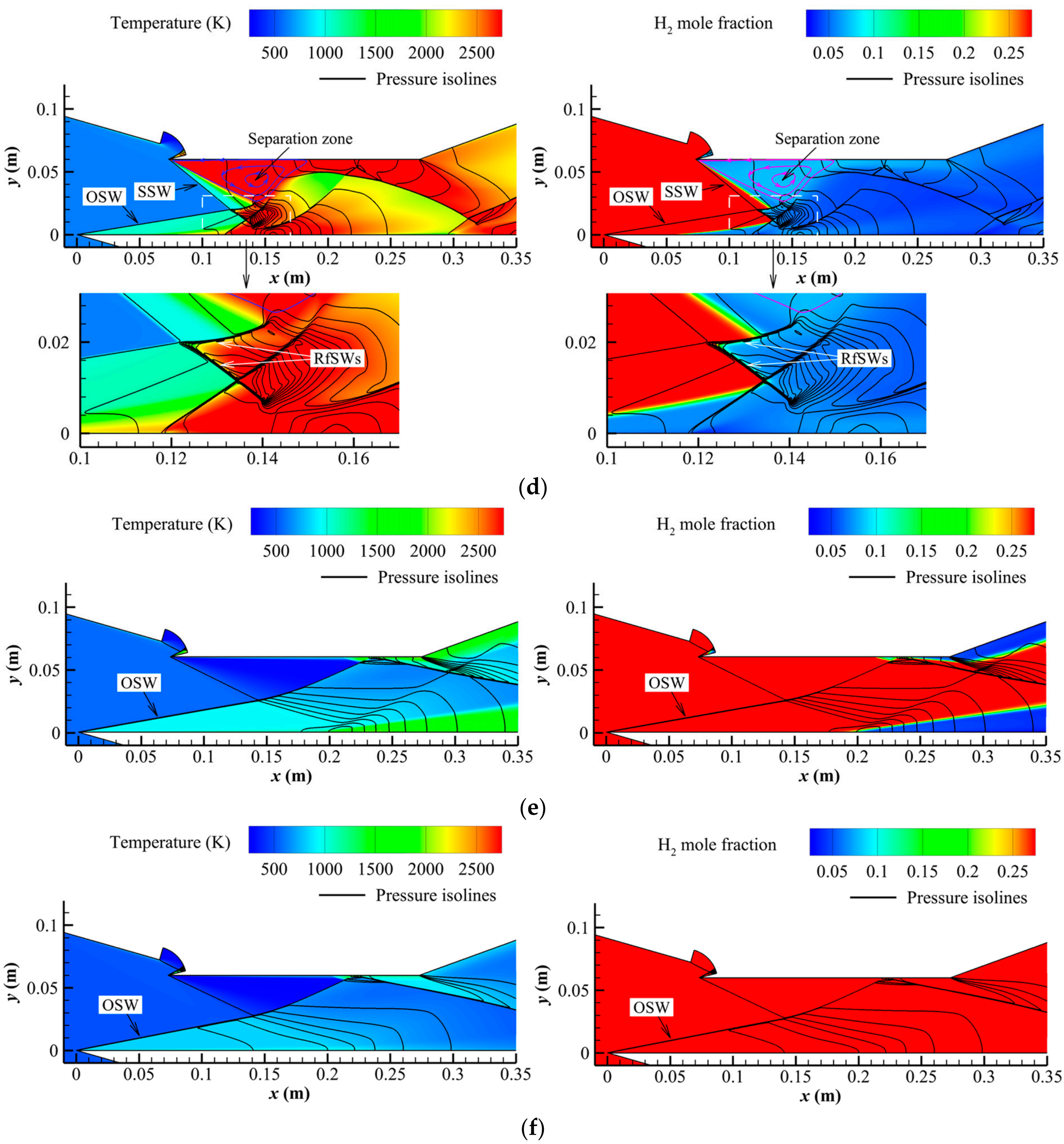

Figure 2. The flow fields in the ODE combustor at different flight Mach numbers without any initiation-assistant measures. (**a**) $Ma_f = 13$ (Case 1). (**b**) $Ma_f = 12$ (Case 2). (**c**) $Ma_f = 11$ (Case 3). (**d**) $Ma_f = 10$ (Case 4). (**e**) $Ma_f = 9$ (Case 5). (**f**) $Ma_f = 8$ (Case 6).

Figure 3 depicts the variation in the theoretical ignition induction length L_{ind} of an ODW as the flight Mach number decreases from $Ma_f = 13$ to 8. L_{ind} is estimated as a product of the ignition delay time τ_{ign} and the post-shock velocity of the OSW V_{s}, i.e., $L_{\mathrm{ind}} = \tau_{\mathrm{ign}} \cdot V_{\mathrm{s}}$, where the ignition delay time τ_{ign} is calculated from the post-shock temperature and pressure of the OSW based on a constant combustion assumption. The OSW–ODW transition lengths L_{tran} evaluated in the simulated cases are also presented in Figure 3 for comparison. As shown, the simulated L_{tran} agrees well with the theoretically predicted L_{ind} in the cases of Ma_f = 11, 12, and 13. At these high flight Mach numbers, both L_{ind} and L_{tran} are on the order of centimeters, which facilitates the transition of the formed OSW into an ODW within a short distance and maintains a significantly high percentage of the oblique detonative combustion mode within the length-limited ODE combustor.

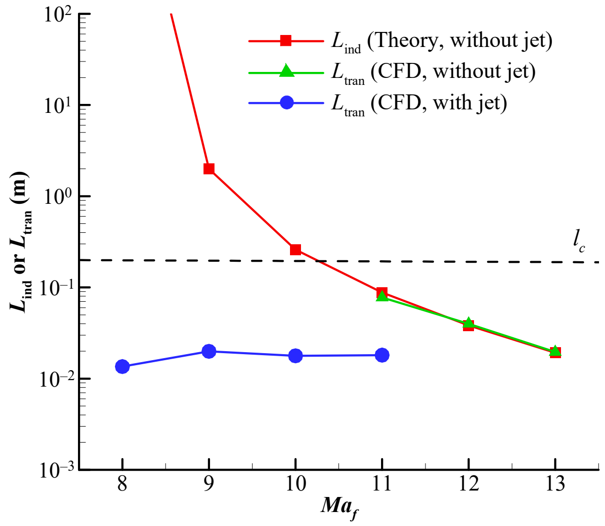

Figure 3. The theoretical ignition induction length L_{ind} and the simulated OSW-ODW transition length L_{tran} as functions of the flight Mach number Ma_f.

However, when the flight Mach number decreases to a relatively low value, for example, Ma_f = 9 or 8, L_{ind} increases significantly and can reach a length to the order of meters, which is so excessively large that a direct transition from the OSW to an ODW within the length-limited combustor is impossible. As a result, the percentage of the detonative combustion mode may be very low, detonative combustion may not occur, or no combustion may occur in the combustor at all. To ensure the stable operations of the ODE within its design range (i.e., $8 \leq Ma_f \leq 13$), certain initiation-assistant measures are necessary to facilitate the rapid initiation of an ODW within the length-limited combustor at low flight Mach numbers, e.g., Ma_f = 8, 9, 10 and even 11.

3.2. *ODW Initiation Characteristics in the Combustor at Different H_f*

Note again that the variation in flight altitude considered here is simply implemented by changing the combustor's inflow pressure as described in Section 2.3. Figure 4 shows the numerical shadowgraphs and the H_2 mole fraction contours (superimposed with pressure isolines) of the flow fields in the combustor without any initiation-assistant measures at different inflow pressures p_i. As indicated in Figure 4a, where $p_i = p_{\text{ref}}$ (the baseline case with Ma_f = 9 and H_f = 30 km), an ODW is quickly initiated, with a relatively short transition length, from the OSW on the cowl side of the combustor. On the body side, a large leading-edge separation is induced, and an SSW is formed, which is also an oblique detonation in this configuration. As a result of the interaction between the ODW and the SSW, a Mach reflection pattern occurs, and a Mach stem (MS) is generated in the middle height of the combustor. As shown, the MS is a detonation wave near-normally inclined to the incoming H_2/air mixture, which actually corresponds to the strong solution of an oblique detonation [11,12]. Therefore, the detonative combustion of the premixed combustible gas occurs in the form of an ODW, an SSW, and an MS in the combustor in this case.

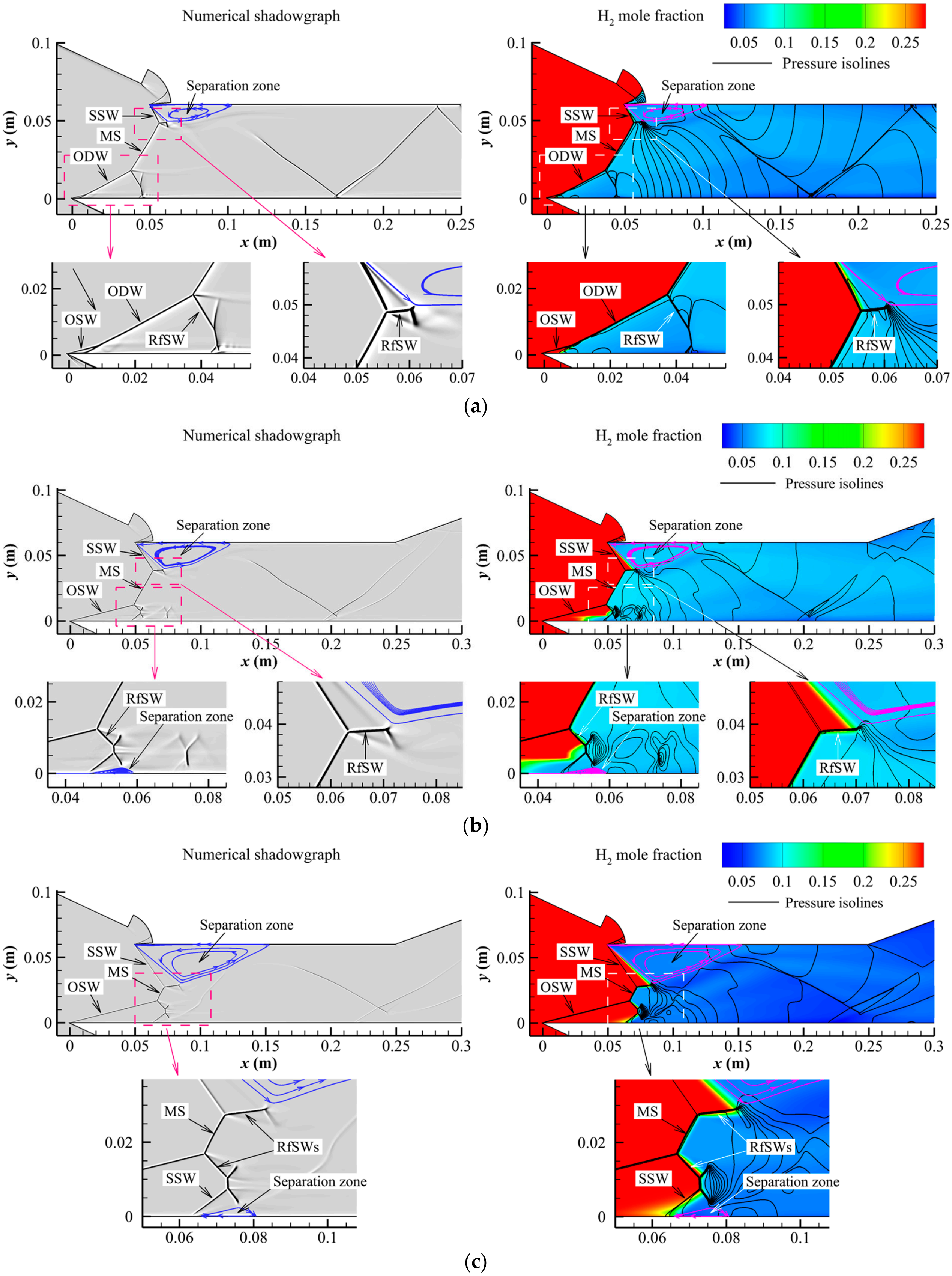

Figure 4. *Cont.*

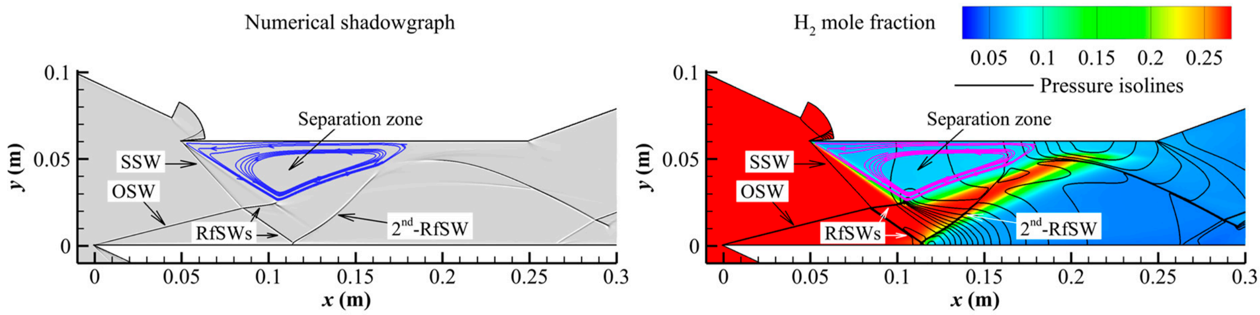

(**d**)

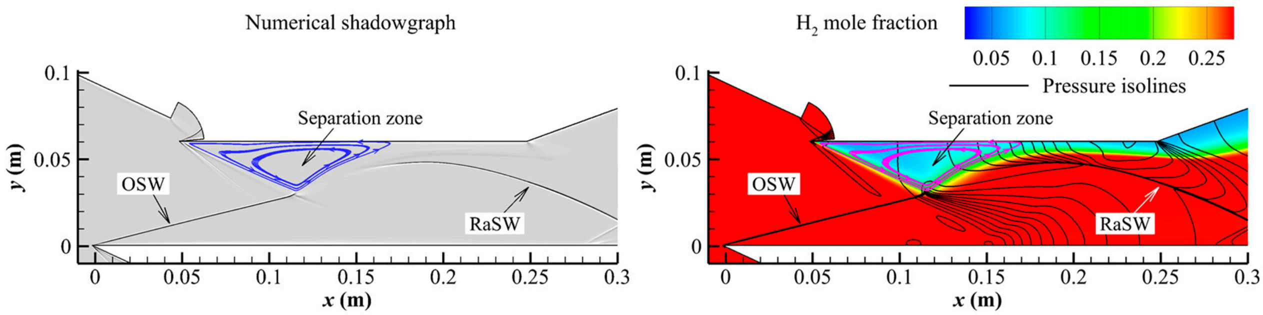

(**e**)

Figure 4. The flow fields in the ODE combustor at different inflow pressures without any initiation-assistant measures. (**a**) $p_i = p_{\mathrm{ref}}$ (Case 11: $H_f = 30$ km). (**b**) $p_i = 0.2\ p_{\mathrm{ref}}$ (Case 12: $H_f = 41$ km). (**c**) $p_i = 0.1\ p_{\mathrm{ref}}$ (Case 13: $H_f = 47$ km). (**d**) $p_i = 0.05\ p_{\mathrm{ref}}$ (Case 14: $H_f = 52$ km). (**e**) $p_i = 0.025\ p_{\mathrm{ref}}$ (Case 15: $H_f = 57$ km).

At $p_i = 0.2\ p_{\mathrm{ref}}$ (Case 12 in Figure 4b, analogous to $H_f = 41$ km), a similar flow pattern with the formation of an MS occurs in the combustor, but the combustion behavior differs from that observed at $p_i = p_{\mathrm{ref}}$ (Figure 4a, Case 11). On the cowl side of the combustor, the OSW fails to transition into an ODW within a short distance in this case because the L_{ind} behind the OSW significantly increases due to the low inflow pressure (as shown in Figure 5). Part of the mixture that passes through the OSW exhibits decoupled combustion downstream, while another part of the mixture exhibits some detonative combustion through the lower RfSW of the Mach reflection pattern. On the body side of the combustor, the formed SSW does not induce significant combustion of the mixture in this case; instead, the corresponding mixture undergoes detonative combustion through the upper RfSW of the Mach reflection pattern. In this middle height of the combustor, due to the higher pressure and temperature behind the MS and the resulting shorter L_{ind} (see Figure 5), the MS again manifests itself as a detonation wave, which dominates the detonative combustion mode in the combustor. In Figure 5, the theoretical ignition induction length of the MS is estimated based on the post-shock flow parameters of a normal shock wave (NSW), a proper approximation of the nature of a strong wave of the MS. Compared to the MS formed in Figure 4a, the length of the MS also slightly decreases in Figure 4b due to the reduced strength of the Mach reflection (between the OSW and the SSW) in the present lower inflow pressure case.

For a lower inflow pressure of $p_i = 0.1\ p_{\mathrm{ref}}$ (Case 13, analogous to $H_f = 47$ km) shown in Figure 4c, detonative combustion of the inflowing mixture still occurs in the combustor through the formed Mach reflection flow pattern, but the length of the MS decreases significantly. Moreover, the OSW no longer directly induces combustion of the mixture over a short distance due to the significant increase in the ignition induction length L_{ind} (see Figure 5); instead, the mixture undergoes detonative combustion through the RfSW of the Mach reflection and a small SSW generated by their interaction with the wall boundary layer. In both cases ($p_i = 0.2\ p_{\mathrm{ref}}$ and $0.1\ p_{\mathrm{ref}}$), although the reduction in the combustor's inflow pressure due to the increase in flight altitude results in a significant decrease in

L_{ind} behind the OSW, the combustor still maintains a great percentage of the detonative combustion mode under the combined effects of the MS and the corresponding RfSWs.

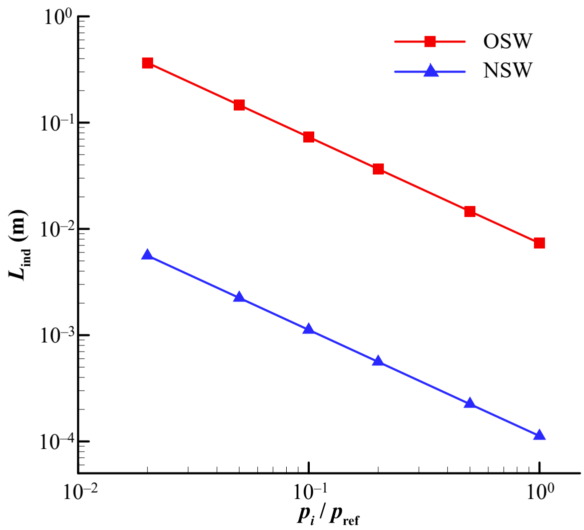

Figure 5. The theoretical ignition induction length L_{ind} as a function of the inflow pressure p_i, calculated from the post-shock flow parameters of an OSW and an NSW.

When the combustor's inflow pressure further decreases to p_i = 0.05 p_{ref} (Case 14, analogous to H_f = 52 km), as shown in Figure 4d, the length of the MS diminishes, and the reflection pattern between the OSW and the SSW appears as a regular pattern. The ignition induction length behind the OSW significantly increases to approximately $L_{\mathrm{ind}} \approx 0.15$ m (see Figure 5), and no combustion is observed behind the OSW. No combustion occurs behind the SSW, and the interaction between the OSW and the SSW does not induce any combustion either. The inflowing mixture only undergoes a decoupled combustion induced by a secondary reflected shock wave (2nd-RfSW) near the cowl wall of the combustor. Overall, no detonative combustion occurs within the present length-limited combustor under this low inflow pressure condition.

As the combustor's inflow pressure finally decreases to p_i = 0.025 p_{ref} (Case 15, analogous to H_f = 57 km), the ignition induction length behind the OSW significantly increases to approximately $L_{\mathrm{ind}} \approx 0.36$ m (see Figure 5), which exceeds the length of the combustor (l_c = 0.2 m or $l_c + d_c$ = 0.25 m). As a result, no combustion occurs behind the OSW, as shown in Figure 4e. The formed SSW is extremely weak in this case, failing to induce any combustion. The only regions where combustion occurs are the large leading-edge separation zone on the body wall and its wake. However, these regions are not within the main flow channel, implying that the majority of the inflowing H_2/air mixture does not burn out before it expands in the nozzle and that the ODE may fail to generate enough thrust in this case. Therefore, certain initiation-assistant measures are required to ensure the normal operations of the ODE under low inflow pressure conditions, i.e., at high flight altitudes.

4. ODW Initiation Assisted by a Transverse Jet

4.1. ODW Initiation at Low Ma_f Assisted by a Transverse Jet

4.1.1. The Transverse-Jet-Assisted Initiation Approach for Wide-Range-Ma_f Applications

According to the analyses in Section 3.1, the main reason for the failure of ODW initiation in the combustor at a low flight Mach number is the excessively low temperature behind the OSW due to insufficient shock compressions, which can subsequently lead to an excessive L_{ind}. The occurrence of detonation is largely delayed in spatial aspects, or even there is an absence of combustion in some cases. Therefore, one important way to facilitate ODW initiation at low flight Mach numbers is to increase the post-shock temperature or to generate some locally high-temperature regions (known as hot spots) without changing the key geometric configuration of the combustor.

At this point, the abrupt initiation structure of a wedge-induced ODW [17,18] can be learned. As shown in Figure 6a, after the compression of the OSW, combustion of the premixed combustible gas begins downstream of the OSW at a certain distance (i.e., L_{ind}). A series of compression waves (also called combustion waves) is generated within the induction zone through the heat release of combustion, propagates downstream, and spatially converges in the meantime. These convergent compression waves interact with the OSW either in a direct way or by forming a weak shock wave to interact with the OSW, leading to the initiation of the ODW.

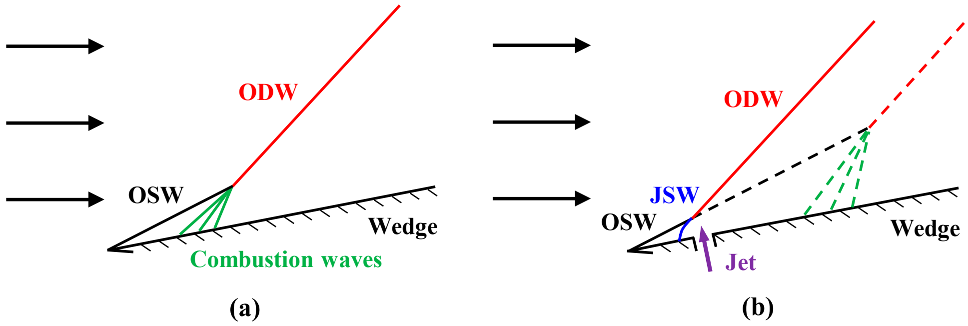

Figure 6. Initiation structures of a wedge-induced ODW: (**a**) abrupted OSW–ODW transition pattern and (**b**) initiation assisted by a transverse jet.

Inspired by such an abrupt mechanism in the natural initiation of an ODW, we propose introducing a transverse jet from the wedge wall (as shown in Figure 6b), which generates a jet shock wave (JSW) within the induction zone. This JSW, replacing the spontaneous compression waves in natural initiation, interacts with the OSW, which is expected to be able to initiate an ODW in advance. With a suitable strength of the transverse jet, such a transverse-jet-assisted measure is expected to be able to control the initiation location of the ODW by adjusting the jet location, especially at low-flight Mach numbers.

The embedding of the transverse jet into the ODE combustor is shown schematically in Figure 7. For the wide-range-Ma_f applications of the ODE, the jet is set on the cowl wall of the combustor and at a distance of L_{jet} = 20 mm downstream from the leading edge, and the width of the transverse jet is set as W_{jet} = 1 mm. For the jet medium, the fuel, i.e., H_2 gas, is chosen based on the following considerations. First, H_2 itself serves as the main consumable carried by aircraft in the fuel tank; hence, utilizing H_2 gas as the jet medium avoids additional structural complexities, such as additional storage devices. Second, H_2 gas has a low density and a high speed of sound. At the same mass flow rate and injection Mach number, the H_2 jet has a higher momentum and a greater penetration depth and produces a stronger JSW than most other gases. Third, the mixing process in the inlet is nonideal in practical ODEs, and the inflowing mixture into the combustor is nonuniform in terms of the equivalence ratio and is always fuel-lean near the walls [48]. In this case, the injected H_2 near the combustor wall can serve as additional fuel to further mix with the unburned air and combust in that region, thereby potentially producing more thrust. However, the mixing process is neglected in the present study; instead, a uniformly premixed stoichiometric H_2/air mixture is employed for simplicity.

Moreover, the H_2 jet Mach number is set to one, and its total temperature is set at 300 K. Then, the mass flow rate of the H_2 jet can be determined based on its total pressure, and vice versa. The mass flow rate of the H_2 jet is characterized using a dimensionless parameter $\Delta\phi_{\text{jet}}$, which is defined as the absolute increment in the total equivalence ratio inside the combustor due to the H_2 jet. For different flight Mach numbers, the employed values of $\Delta\phi_{\text{jet}}$, the corresponding total pressures $p_{0,\text{jet}}$ of the H_2 jet, and the corresponding jet-to-crossflow momentum ratio $J = \rho_{\text{jet}} V_{\text{jet}}^2 / \rho_s V_s^2$ are summarized in Table 1 (Cases 7–10). Here, ρ_{jet} and V_{jet} are the density and velocity magnitude of the H_2 jet, respectively, and ρ_s

is the post-shock density of the OSW. As can be seen in Table 1, the required jet-to-crossflow momentum ratio increases when the flight Mach number decreases due to greater difficulty with detonation initiation at a lower flight Mach number.

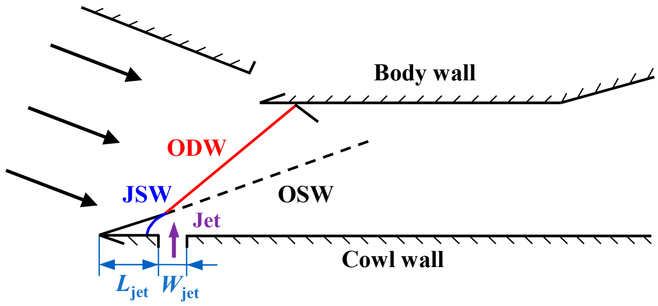

Figure 7. Schematic of the ODE combustor with a transverse H_2 jet for a wide-range-Ma_f application.

4.1.2. Numerical Validations of Transverse-Jet-Assisted ODW Initiation at Low Ma_f

Figure 8 illustrates the combustion flow fields in the combustor at Ma_f = 11, 10, 9, and 8 when a transverse H_2 jet is utilized on the cowl wall as described in Section 4.1.1. For comparison, the simulated OSW–ODW transition lengths L_{tran} with the transverse H_2 jet employed are also summarized in Figure 3. As shown, the transverse H_2 jet helps to initiate an ODW from the OSW in advance at Ma_f = 11, with the simulated L_{tran} reducing from approximately 0.1 m to 0.02 m, which is also demonstrated in a comparison between Figures 2c and 8a. At Ma_f = 10, although detonative combustion occurs, the OSW fails to transition to an ODW within the length-limited combustor without the jet, as described in Section 3.1. Now, with the transverse H_2 jet employed, the OSW transitions to an ODW rapidly with a simulated L_{tran} of approximately 0.02 m (see Figure 8b), which is reduced significantly (by an order of magnitude) compared to the theoretical L_{ind} predicted without the jet (as shown in Figure 3).

At Ma_f = 9, the no detonation initiation case without the jet, an ODW is successfully initiated from the OSW with a simulated $L_{tran} \approx 0.02$ m by employing the transverse H_2 jet (as shown in Figure 8c), which facilitates oblique detonative combustion in the combustor. As indicated in Figure 3, the simulated L_{tran} with the jet at this Ma_f = 9 is reduced by approximately two orders of magnitude compared to the corresponding theoretical L_{ind} predicted without the jet. At Ma_f = 8, the case without combustion in the core flow when there is no jet, an ODW is also successfully formed with the effects of the jet, and hence, the main mode occurring in the combustor is again the oblique detonative combustion (as shown in Figure 8d). Moreover, Figure 3 reveals that the reduction in the simulated L_{tran} using the jet from the theoretical L_{ind} without the jet is more than four orders of magnitude at this Ma_f = 8, and the simulated L_{tran} ($\approx$0.02 m) is ultimately within the length scales of the combustor (l_c = 0.2 m or $l_c + d_c$ = 0.273 m).

In summary, with the effects of the transverse H_2 jet, an ODW is successfully initiated within the combustor at all low-flight Mach numbers from 8 to 11, indicating the occurrence of oblique detonative combustion for the majority of the inflowing combustible mixture into the combustor. In other words, the employment of a transverse jet in the combustor makes the engine capable of operating normally in the whole designed range of flight Mach numbers, i.e., Ma_f = 8 to 13. Furthermore, with the use of the transverse H_2 jet, the transition from the OSW to an ODW occurs at a relatively fixed position at different flight Mach numbers, which is approximately at the designed injection location of the jet, i.e., $L_{tran} \approx L_{jet}$ = 0.02 m. In other words, the initiation location of an ODW in the length-limited ODE combustor can be easily controlled by the injection location of the transverse jet, which is of practical value.

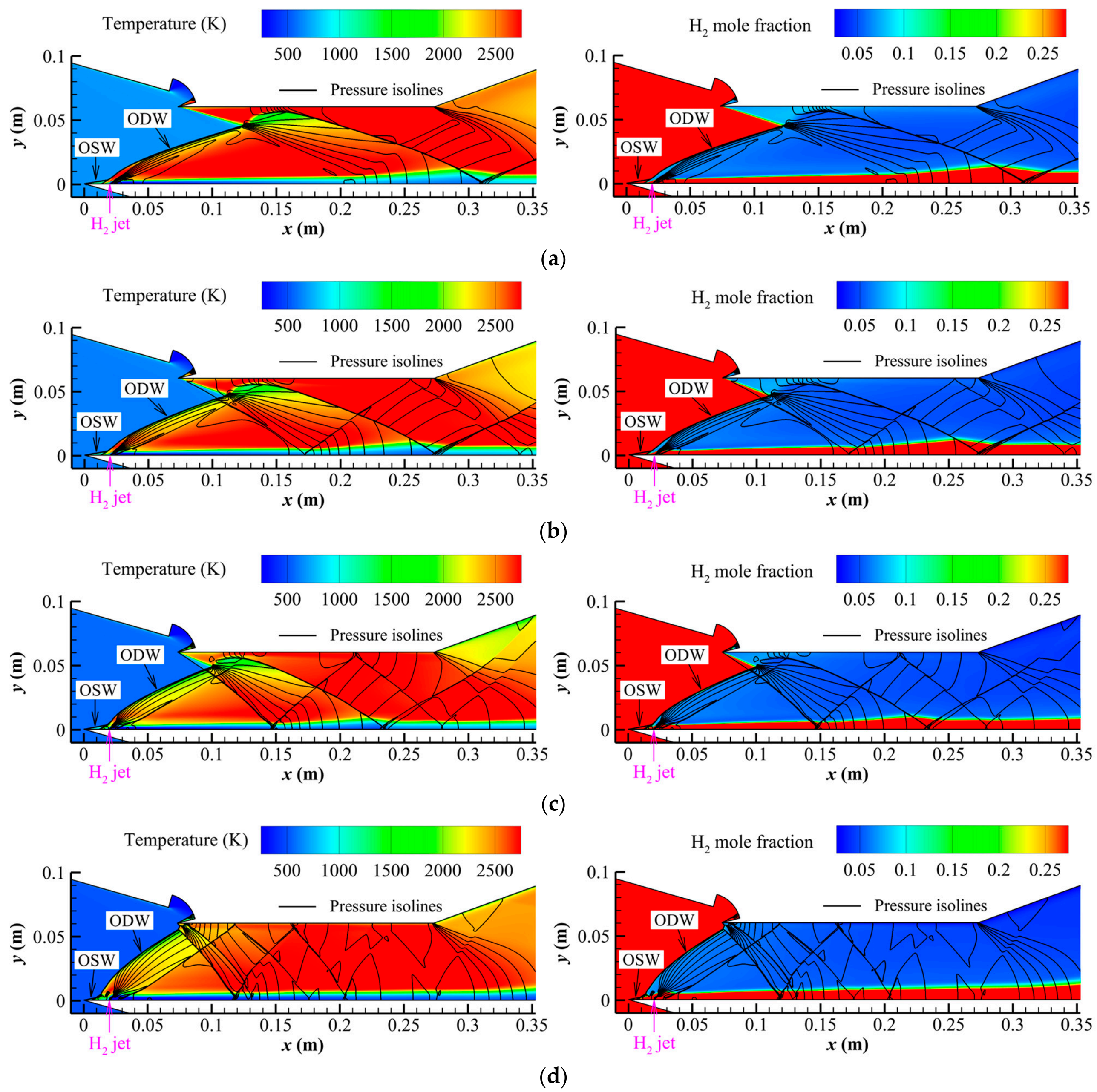

Figure 8. The flow fields in the ODE combustor with a transverse H_2 jet. (**a**) $Ma_f = 11$ and $\Delta\phi_{\text{jet}} = 0.05$. (**b**) $Ma_f = 10$ and $\Delta\phi_{\text{jet}} = 0.05$. (**c**) $Ma_f = 9$ and $\Delta\phi_{\text{jet}} = 0.05$. (**d**) $Ma_f = 8$ and $\Delta\phi_{\text{jet}} = 0.075$.

4.2. ODW Initiation at a High H_f Assisted by a Transverse Jet

4.2.1. The Transverse-Jet-Assisted Initiation Approach for Wide-Range-H_f Applications

The analyses in Section 3.2 reveal that the combustor's inflow pressure p_i decreases near-exponentially as the flight altitude H_f increases, and consequently, the predicted ignition delay time τ_{ign} and the ignition induction length L_{ind} behind the OSW increase near-exponentially as well. The large L_{ind} prevents the OSW–ODW transition in a short distance and indicates a failure of ODW initiation in the length-limited ODE combustor. In this case, an MS generated through the shock/shock interaction between the OSW and the SSW within the space-confined combustor serves as a crucial factor in triggering detonative combustion in the combustor, as shown in Figure 4b (Case 12) and Figure 4c (Case 13). With the strong compression of the MS, L_{ind} can be reduced by approximately two orders of magnitude compared to that with the compression of an OSW (as shown in Figure 5).

This reduction in L_{ind} enables combustion of the mixture to occur over a shorter distance, which, in turn, sustains the presence of the MS, resulting in a tight coupling between the shock wave and the flame, i.e., detonative combustion. However, when the flight altitude further increases and the inflow pressure further decreases, the SSW may become weak enough that the interaction between the OSW and the SSW fails to induce the formation of a Mach reflection pattern, and hence, detonative combustion (as shown in Figure 4c) or even normal combustion (as shown in Figure 4d) does not ultimately occur.

Therefore, an intuitional idea to achieve detonative combustion at high flight altitudes or low inflow pressures is to increase the strength of the SSW using some assistant measures, and a transverse jet could be the way to achieve this. That is, a transverse jet is introduced within the leading-edge separation zone on the body wall to produce a strong JSW, which interacts with the OSW to reactivate a Mach reflection pattern in the combustor, as schematically shown in Figure 9. Then, detonative combustion can be achieved through the MS and its RfSWs in a similar way as shown in Figure 4c,d. Notably, due to the low pressure, density, and velocity within the leading-edge separation zone, a not-very-strong jet is expected to penetrate deep enough to form a suitable JSW. Specifically, the jet is located at a distance of L_{jet} = 10 mm downstream from the combustor's leading edge on the body wall, and the width of the jet is W_{jet} = 2 mm. The fuel, i.e., the H_2 gas, is again chosen as the jet medium, following similar considerations as in Section 4.1.1. The injection Mach number of the jet is set to unity (sonic) with a total temperature of 300 K. The injection total pressure is determined by the mass flow rate, and the latter is nondimensionally expressed by $\Delta\phi_{\text{jet}}$, which is equal to 0.2 in this case. The corresponding jet-to-crossflow momentum ratio $J = \rho_{\text{jet}} V_{\text{jet}}^2 / \rho_i V_i^2$ is equal to 1.73, where ρ_i is the inflow density. Notably, the inflow is assumed as the crossflow in the evaluation of J in the configuration of Figure 9.

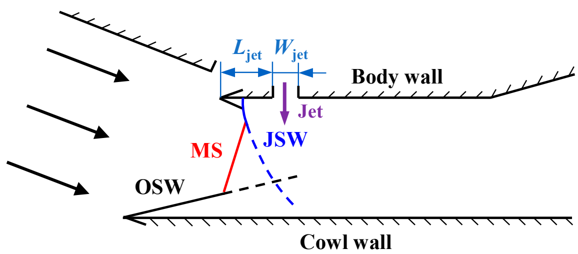

Figure 9. Schematic of the ODE combustor with a transverse H_2 jet for a wide-range-H_f application.

4.2.2. Numerical Validations of Transverse-Jet-Assisted Detonation Initiation at High H_f

To validate the effectiveness of the proposed transverse H_2 jet at high flight altitudes or low inflow pressures, the worst case of p_i = 0.025 p_{ref} (H_f = 57 km) is taken as an example, i.e., Case 16 in Table 2. Figure 10 is a series of numerical shadowgraphs of the flow field in the combustor at different time instances after the introduction of the transverse H_2 jet, which depicts the process of detonation initiation induced by the jet. The two streamlines emitted from the two ends of the injection slot and the H_2 mole fraction isolines of 0.99 are also provided in the numerical shadowgraphs, which synergistically represent the shape and the flow path of the H_2 jet. The initial flow field in the combustor is a steady one without the presence of the jet, as shown in Figure 4e (Case 15) in Section 3.2, and the transverse H_2 jet begins to inject from the designed slot at t = 0. As indicated in Figure 10a, a JSW is generated near the body-wall leading edge of the combustor when the transverse H_2 jet is injected into the separation zone at t = 0.01 ms. At t = 0.07 ms (as shown in Figure 10b), the JSW is almost established and interacts with the incident OSW, forming a regular reflection flow pattern. At this moment, in addition to the formation of the aforementioned JSW, a weaker secondary jet shock wave (2nd-JSW) is generated within the jet.

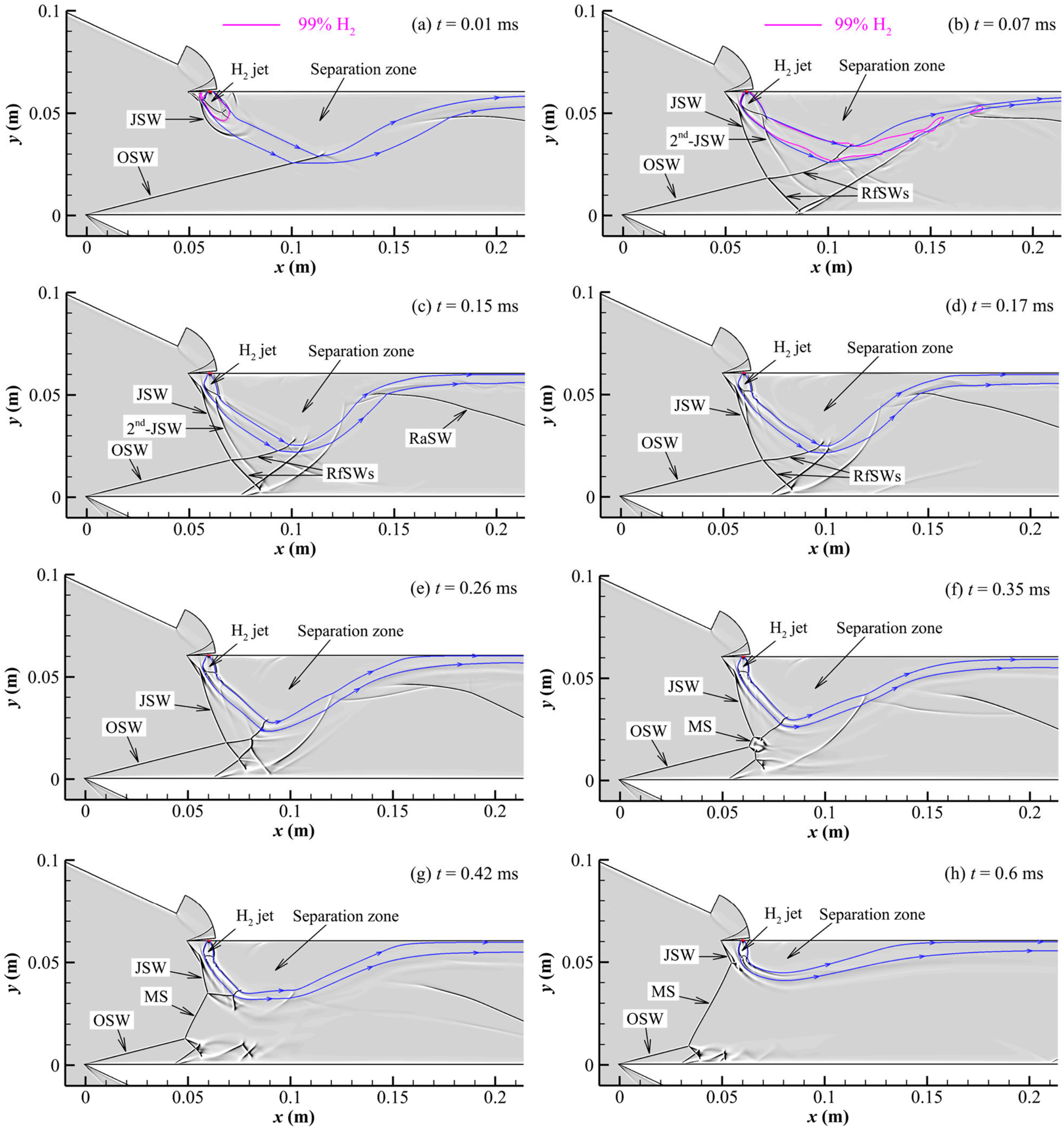

Figure 10. The establishment process of the flow field (numerical shadowgraph) in the ODE combustor with a transverse H_2 jet (p_i = 0.025 p_{ref}, Case 16).

At t = 0.15 ms, the RfSW of the incident OSW interacts with the boundary layer on the cowl wall and induces a small-scale flow separation, forming typical flow separation structures including a separation zone, a separated shock, a reflected shock, and a reattached shock wave, as shown in Figure 10c. Then, the formed 2nd-JSW strengthens and moves upstream gradually, and finally, at t = 0.17 ms, it merges with and enhances the JSW, as shown in Figure 10d. With the strengthening of the JSW, the RfSW of the incident OSW also strengthens correspondingly, leading to an intensified boundary layer separation on the cowl wall of the combustor, as shown in Figure 10e. Subsequently, under the complex interaction of various RfSWs, the regular reflection between the OSW and the JSW transitions to a Mach reflection pattern at t = 0.35 ms, and an MS is formed, as shown in Figure 10f. The formed MS grows and moves upstream gradually (Figure 10g). Ultimately, the MS reaches a steady state, as shown in Figure 10h. During this process, the size of the leading-edge separation zone on the body wall of the combustor reduces gradually and eventually reaches a steady state.

Figure 11 depicts the contours of temperature and H_2 mole fraction (superimposed by pressure isolines) of the ultimately stable flow field in the combustor at t = 1 ms. After introducing the transverse H_2 jet, the simulated L_{ind} is significantly reduced under the influence of the formed MS and its RfSWs, and rapid combustion of the combustible mixture flowing into the combustor occurs, with the combustion products reaching a temperature exceeding 2500 K, implying a stable detonative combustion mode in the combustor. This effect is further confirmed by examining the distributions of various flow parameters along a streamline passing through the MS, as shown in Figure 12. With a rapid increase in pressure, H_2 is rapidly consumed. In other words, the flame is tightly coupled with the shock front, and hence, the formed MS is an overdriven detonation wave. This example demonstrates that with the use of a transverse H_2 jet into the leading-edge separation zone on the body wall, an MS is formed through the interaction between the JSW and the OSW, and stable detonative combustion of the inflowing mixture occurs in the combustor under the effects of the MS and its RfSWs, which allows the ODE to be operated normally even under low-pressure conditions at a high flight altitude.

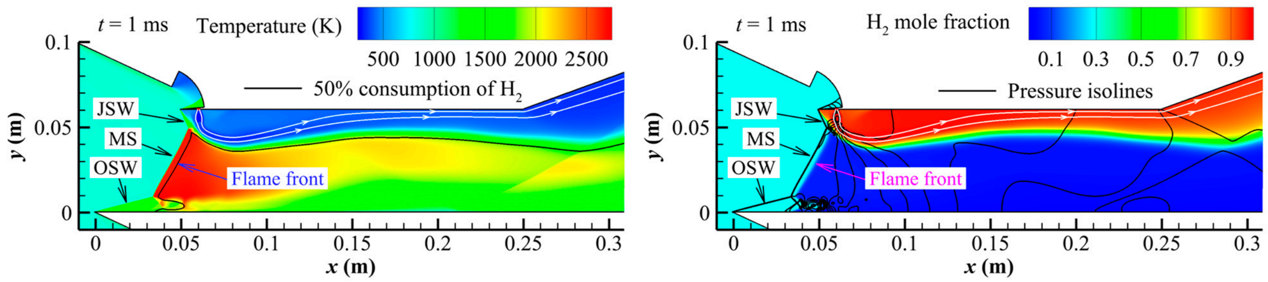

Figure 11. The stable flow field in the ODE combustor with a transverse H_2 jet at t = 1 ms (p_i = 0.025 p_{ref}, Case 16).

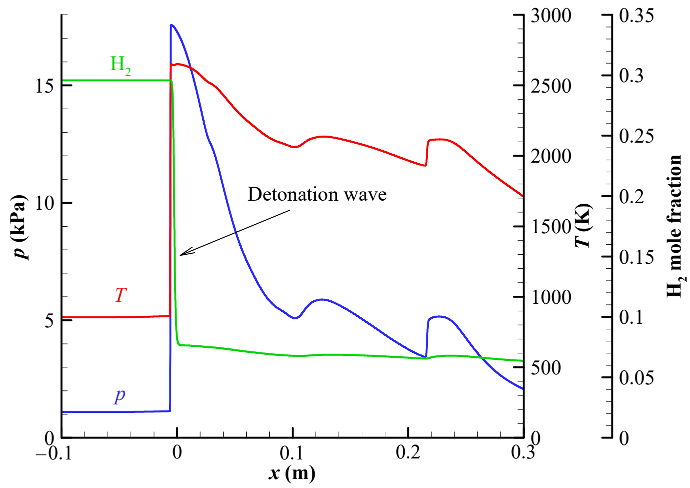

Figure 12. The flow parameter distributions along the streamline that crosses the middle point of the MS at t = 1 ms (p_i = 0.025 p_{ref}, Case 16).

5. Conclusions

Initiation of an ODW in the combustor is a crucial process during the successful operation of an ODE. An ODE designed to be operated over wide ranges of flight Mach numbers and altitudes typically faces detonation initiation issues under certain off-design conditions, which indeed require effective initiation-assistant measures. In this study, numerical simulations were conducted to investigate the initiation characteristics of two

H_2-fueled ODE combustors designed for wide-range flight Mach numbers Ma_f and flight altitudes H_f by solving the 2-D multispecies reactive RANS equations closed by the SST k-ω turbulence model and the modified Jachimowski's H_2/air combustion model.

For an ODE combustor designed for a range of Ma_f = 8 to 13, detonative combustion does not occur in the combustor at the low Ma_f of 8 and 9 without any initiation-assistant measures, and detonative combustion occurs with a low percentage at Ma_f = 10 and 11. With a theoretical analysis, the results show that the failure of detonation in the combustor is caused by the insufficient compression of the OSW at low Ma_f, leading to a significant decrease in the post-shock temperature and a great increase in L_{ind}. Based on the abrupt OSW–ODW transition pattern, a transverse H_2 jet is introduced within the induction zone to generate a JSW to initiate an ODW through a shock/shock interaction. The simulation results show that, assisted by the transverse jet, ODW initiation is successful at all low Ma_f = 8 to 11, and the initiation location is relatively fixed and determined by the jet location.

For the ODE combustor designed for a range of H_f = 30 km to 57 km, failure of detonation is identified at $H_f \geq 52$ km without any initiation-assistant measures. This detonation failure mainly occurs because of the rapid decrease in the combustor's inflow pressure at high H_f, which results in a significant increase in L_{ind}. The formation of an MS is beneficial to the occurrence of detonative combustion at a moderately high H_f where the OSW–ODW transition fails. Therefore, a transverse H_2 jet is introduced within the leading-edge separation zone on the body wall of the combustor at very high H_f, which generates a JSW to enhance the SSW and to make its interaction with the OSW transition into a Mach reflection pattern. Finally, detonative combustion is expected to be achieved through the formed MS and its RfSW. Considering the highest altitude H_f = 57 km as an example, the effectiveness of the transverse jet in detonation initiation is validated by numerical simulation.

This study demonstrates the concept of using a transverse jet to assist detonation initiation within a length-limited ODE combustor at off-design conditions for ODEs operating at wide-range Ma_f and H_f, which is of practical value to the future development of ODEs. Although two jet configurations are proposed to solve the initiation issues encountered at low Ma_f or high H_f, a combination of these two jet configurations is expected to work for a wide-range ODE with a specific flight envelope where Ma_f and H_f vary accordingly. Furthermore, numerical simulations with imperfect inflow conditions such as mixing nonuniformity could be studied in the future to consider the effectiveness of the transverse jet under more practical conditions and to carry out necessary optimizations.

Author Contributions: Conceptualization, Z.Z.; methodology, Z.Z.; validation, Z.Z. and Z.J.; formal analysis, Z.Z. and Z.J.; investigation, Z.Z. and Z.J.; writing—original draft preparation, Z.J.; writing—review and editing, Z.Z. and Z.J.; supervision, Z.Z.; project administration, Z.Z.; funding acquisition, Z.Z. All authors have read and agreed to the published version of the manuscript.

Funding: This research was supported by the National Natural Science Foundation of China (No. 12202374). The authors thank the Institute of Mechanics, Chinese Academy of Sciences for providing the computational resources.

Data Availability Statement: Data will be available on request.

Conflicts of Interest: The authors declare no conflict of interest.

Nomenclature

List of Symbols

d_c	Upstream-extending distance of cowl's leading edge (m).
h_c	Height of combustor (m).
H_f	Flight altitude (m).
J	Jet-to-crossflow momentum ratio.
l_c	Length of combustor (m).
L_{ind}	Ignition induction length (m).

L_{jet}	Distance of jet downstream from wall's leading edge (m).
L_{tran}	Oblique shock wave to oblique detonation wave transition length (m).
Ma_f	Flight Mach number.
$p_{0,\text{jet}}$	Total pressure of jet (Pa).
p_i	Inflow pressure (Pa).
p_{ref}	Reference inflow pressure in baseline case (Pa).
T_i	Inflow temperature (K).
T_{ref}	Reference inflow temperature in baseline case (K).
V_i	Inflow velocity magnitude (m/s).
V_{jet}	Velocity magnitude of jet (m/s).
V_{ref}	Reference inflow velocity magnitude in baseline case (m/s).
V_{s}	Post-shock velocity magnitude (m/s).
W_{jet}	Width of transverse jet (m).
$\Delta\phi_{\text{jet}}$	Increment in total equivalence ratio by fuel jet.
θ_i	Inclined angle of inlet wall (°).
ρ_i	Inflow density (kg/m^3).
ρ_{jet}	Density of jet (kg/m^3).
ρ_{s}	Post-shock density (kg/m^3).
τ_{ign}	Ignition delay time (s).
Abbreviation	
2-D	Two-dimensional.
2nd-JSW	Secondary jet shock wave.
2nd-RfSW	Secondary reflected shock wave.
3-D	Three-dimensional.
HLLC	Harten–Lax–van Leer contact.
JSW	Jet shock wave.
MS	Mach stem.
NSW	Normal shock wave.
ODE	Oblique detonation engine.
ODW	Oblique detonation wave.
OSW	Oblique shock wave.
RANS	Reynolds-averaged Navier–Stokes.
RaSW	Reattachment shock wave.
RfSW	Reflected shock wave.
SST	Shear-stress transport.
SSW	Separated shock wave.
TVD	Total variation diminishing.

References

1. Sziroczak, D.; Smith, H. A Review of Design Issues Specific to Hypersonic Flight Vehicles. *Prog. Aerosp. Sci.* **2016**, *84*, 1–28. [CrossRef]
2. Liu, Q.; Baccarella, D.; Lee, T. Review of Combustion Stabilization for Hypersonic Airbreathing Propulsion. *Prog. Aerosp. Sci.* **2020**, *119*, 100636. [CrossRef]
3. Mcclinton, C. High Speed/Hypersonic Aircraft Propulsion Technology Development. In *Advances on Propulsion Technology for High-Speed Aircraft*; RTO: Neuilly-sur-Seine, France, 2008.
4. Oehlschlaeger, M.A. Grand Challenges in Aerospace Propulsion. *Front. Aerosp. Eng.* **2022**, *1*, 1027943. [CrossRef]
5. Jiang, Z.; Zhang, Z.; Liu, Y.; Wang, C.; Luo, C. Criteria for Hypersonic Airbreathing Propulsion and Its Experimental Verification. *Chin. J. Aeronaut.* **2021**, *34*, 94–104. [CrossRef]
6. Rosato, D.A.; Thornton, M.; Sosa, J.; Bachman, C.; Goodwin, G.B.; Ahmed, K.A. Stabilized Detonation for Hypersonic Propulsion. *Proc. Natl. Acad. Sci. USA* **2021**, *118*, e2102244118. [CrossRef] [PubMed]
7. Higgins, A.J. Ram Accelerators: Outstanding Issues and New Directions. *J. Propuls. Power* **2006**, *22*, 1170–1187. [CrossRef]
8. Braun, E.M.; Lu, F.K.; Wilson, D.R.; Camberos, J.A. Airbreathing Rotating Detonation Wave Engine Cycle Analysis. *Aerosp. Sci. Technol.* **2013**, *27*, 201–208. [CrossRef]
9. Wolański, P. Detonative Propulsion. *Proc. Combust. Inst.* **2013**, *34*, 125–158. [CrossRef]
10. Dudebout, R.; Sislian, J.P.; Oppitz, R. Numerical Simulation of Hypersonic Shock-Induced Combustion Ramjets. *J. Propuls. Power* **1998**, *14*, 869–879. [CrossRef]
11. Zhang, Z.; Wen, C.; Yuan, C.; Liu, Y.; Han, G.; Wang, C.; Jiang, Z. An Experimental Study of Formation of Stabilized Oblique Detonation Waves in a Combustor. *Combust. Flame* **2022**, *237*, 111868. [CrossRef]

12. Han, X.; Liu, Y.; Zhang, Z.; Zhang, W.; Yuan, C.; Han, G.; Jiang, Z. Experimental Demonstration of Forced Initiation of Kerosene Oblique Detonation by an On-Wedge Trip in an ODE Model. *Combust. Flame* **2023**, *258*, 113102. [CrossRef]
13. Sterling, J.; Cummings, E.; Ghorbanian, K.; Pratt, D.; Sobota, T.; Brock, N.; Brown, M.; Segall, J.; DeBarber, P. Oblique Detonation Wave Studies in the Caltech T-5 Shock Tunnel Facility. In Proceedings of the 8th AIAA International Space Planes and Hypersonic Systems and Technologies Conference, Norfolk, VA, USA, 27–30 April 1998; American Institute of Aeronautics and Astronautics: Reston, VA, USA, 1998.
14. Li, C.; Kailasanath, K.; Oran, E.S. Detonation Structures behind Oblique Shocks. *Phys. Fluids* **1994**, *6*, 1600–1611. [CrossRef]
15. Viguier, C.; da Silva, L.F.F.; Desbordes, D.; Deshaies, B. Onset of Oblique Detonation Waves: Comparison between Experimental and Numerical Results for Hydrogen-Air Mixtures. *Symp. Int. Combust.* **1996**, *26*, 3023–3031. [CrossRef]
16. Lin, Z.; Zhang, J.; Zhou, J. Design of High-Enthalpy Premixed Supersonic Heater and Experimental Study of Detonation. In Proceedings of the 43rd AIAA/ASME/SAE/ASEE Joint Propulsion Conference & Exhibit, Cincinnati, OH, USA, 8–11 July 2007; American Institute of Aeronautics and Astronautics: Reston, VA, USA, 2007.
17. Teng, H.H.; Jiang, Z.L. On the Transition Pattern of the Oblique Detonation Structure. *J. Fluid Mech.* **2012**, *713*, 659–669. [CrossRef]
18. Teng, H.; Tian, C.; Zhang, Y.; Zhou, L.; Ng, H.D. Morphology of Oblique Detonation Waves in a Stoichiometric Hydrogen–Air Mixture. *J. Fluid Mech.* **2021**, *913*, A1. [CrossRef]
19. Liu, Y.; Wu, D.; Yao, S.; Wang, J. Analytical and Numerical Investigations of Wedge-Induced Oblique Detonation Waves at Low Inflow Mach Number. *Combust. Sci. Technol.* **2015**, *187*, 843–856. [CrossRef]
20. Yang, P.; Teng, H.; Jiang, Z.; Ng, H.D. Effects of Inflow Mach Number on Oblique Detonation Initiation with a Two-Step Induction-Reaction Kinetic Model. *Combust. Flame* **2018**, *193*, 246–256. [CrossRef]
21. Bian, J.; Zhou, L.; Teng, H. Structural and Thermal Analysis on Oblique Detonation Influenced by Different Forebody Compressions in Hydrogen-Air Mixtures. *Fuel* **2021**, *286*, 119458. [CrossRef]
22. Zhang, Y.; Fang, Y.; Ng, H.D.; Teng, H. Numerical Investigation on the Initiation of Oblique Detonation Waves in Stoichiometric Acetylene–Oxygen Mixtures with High Argon Dilution. *Combust. Flame* **2019**, *204*, 391–396. [CrossRef]
23. Wang, T.; Zhang, Y.; Teng, H.; Jiang, Z.; Ng, H.D. Numerical Study of Oblique Detonation Wave Initiation in a Stoichiometric Hydrogen-Air Mixture. *Phys. Fluids* **2015**, *27*, 096101. [CrossRef]
24. Teng, H.; Ng, H.D.; Jiang, Z. Initiation Characteristics of Wedge-Induced Oblique Detonation Waves in a Stoichiometric Hydrogen-Air Mixture. *Proc. Combust. Inst.* **2017**, *36*, 2735–2742. [CrossRef]
25. Fang, Y.; Hu, Z.; Teng, H. Numerical Investigation of Oblique Detonations Induced by a Finite Wedge in a Stoichiometric Hydrogen-Air Mixture. *Fuel* **2018**, *234*, 502–507. [CrossRef]
26. Xiang, G.X.; Gao, X.; Tang, W.J.; Jie, X.Z.; Huang, X. Numerical Study on Transition Structures of Oblique Detonations with Expansion Wave from Finite-Length Cowl. *Phys. Fluids* **2020**, *32*, 056108. [CrossRef]
27. Zhang, G.Q.; Gao, S.F.; Xiang, G.X. Study on Initiation Mode of Oblique Detonation Induced by a Finite Wedge. *Phys. Fluids* **2021**, *33*, 016102. [CrossRef]
28. Xiang, G.; Li, X.; Sun, X.; Chen, X. Investigations on Oblique Detonations Induced by a Finite Wedge in High Altitude. *Aerosp. Sci. Technol.* **2019**, *95*, 105451. [CrossRef]
29. Maeda, S.; Kasahara, J.; Matsuo, A. Oblique Detonation Wave Stability around a Spherical Projectile by a High Time Resolution Optical Observation. *Combust. Flame* **2012**, *159*, 887–896. [CrossRef]
30. Maeda, S.; Sumiya, S.; Kasahara, J.; Matsuo, A. Initiation and Sustaining Mechanisms of Stabilized Oblique Detonation Waves around Projectiles. *Proc. Combust. Inst.* **2013**, *34*, 1973–1980. [CrossRef]
31. Fang, Y.; Zhang, Z.; Hu, Z.; Deng, X. Initiation of Oblique Detonation Waves Induced by a Blunt Wedge in Stoichiometric Hydrogen-Air Mixtures. *Aerosp. Sci. Technol.* **2019**, *92*, 676–684. [CrossRef]
32. Gong, J.S.; Zhang, Y.; Pan, H.; Jia, B.; Meng, H.; Lin, X. Experimental Investigation on Initiation of Oblique Detonation Waves. In Proceedings of the 21st AIAA International Space Planes and Hypersonics Technologies Conference, Xiamen, China, 6–9 March 2017; American Institute of Aeronautics and Astronautics: Reston, VA, USA, 2017.
33. Qin, Q.; Zhang, X. A Novel Method for Trigger Location Control of the Oblique Detonation Wave by a Modified Wedge. *Combust. Flame* **2018**, *197*, 65–77. [CrossRef]
34. Teng, H.; Zhang, Y.; Yang, P.; Jiang, Z. Oblique Detonation Wave Triggered by a Double Wedge in Hypersonic Flow. *Chin. J. Aeronaut.* **2022**, *35*, 176–184. [CrossRef]
35. Bomjan, B.; Bhattrai, S.; Tang, H. Characterization of Induction and Transition Methods of Oblique Detonation Waves over Dual-Angle Wedge. *Aerosp. Sci. Technol.* **2018**, *82–83*, 394–401. [CrossRef]
36. Xiang, G.; Zhang, Y.; Tu, Q.; Gao, Y.; Huang, X.; Peng, T. The Initiation Characteristics of Oblique Detonation Waves Induced by a Curved Surface. *Aerosp. Sci. Technol.* **2022**, *128*, 107743. [CrossRef]
37. Xiong, H.; Qiu, R.; Han, X.; Yan, H.; You, Y. Investigating the Flow Characteristics and Thermodynamic Performance of Curved Detonation Waves. *Phys. Fluids* **2023**, *35*, 087119. [CrossRef]
38. Han, X.; Zhang, W.-S.; Zhang, Z.-J.; Liu, Y.-F.; Jiang, Z.-L. Numerical Study of Oblique Detonation Waves Induced by a Bump. *Tuijin Jishu/J. Propuls. Technol.* **2022**, *43*, 185–196. [CrossRef]
39. Xiang, G.; Zhang, Y.; Zhang, C.; Kou, Y. Study on Initiation Mechanism of Oblique Detonation Induced by Blunt Bump on Wedge Surface. *Fuel* **2022**, *323*, 124314. [CrossRef]

40. Lei, Q.; Zhao, X.; Zheng, J.; He, J.; Wang, K.; Fan, W. Role of Overdriven State of Ignition Wave in Pre-Detonators on Detonation Transition Modes in a Flat Chamber. *Aerosp. Sci. Technol.* **2021**, *115*, 106771. [CrossRef]
41. Yang, C.; Wu, X.; Ma, H.; Peng, L.; Gao, J. Experimental Research on Initiation Characteristics of a Rotating Detonation Engine. *Exp. Therm. Fluid Sci.* **2016**, *71*, 154–163. [CrossRef]
42. Han, X.; Zhou, J.; Lin, Z.-Y. Experimental Investigations of Detonation Initiation by Hot Jets in Supersonic Premixed Flows. *Chin. Phys. B* **2012**, *21*, 124702. [CrossRef]
43. Cai, X.; Liang, J.; Lin, Z.; Deiterding, R.; Liu, Y. Parametric Study of Detonation Initiation Using a Hot Jet in Supersonic Combustible Mixtures. *Aerosp. Sci. Technol.* **2014**, *39*, 442–455. [CrossRef]
44. Cai, X.; Liang, J.; Deiterding, R. Numerical Investigation on Detonation Control Using a Pulse Hot Jet in Supersonic Combustible Mixture. *Combust. Sci. Technol.* **2016**, *188*, 1674–1690. [CrossRef]
45. Yao, J.; Lin, Z. Numerical Investigation of Jet-Wedge Combinatorial Initiation for Oblique Detonation Wave in Supersonic Premixed Mixture. *Phys. Fluids* **2023**, *35*, 026101. [CrossRef]
46. Zhang, Z.; Liu, Y.; Wen, C. Mechanisms of the Destabilized Mach Reflection of Inviscid Oblique Detonation Waves before an Expansion Corner. *J. Fluid Mech.* **2022**, *940*, A29. [CrossRef]
47. Zhang, Z.; Wen, C.; Zhang, W.; Liu, Y.; Jiang, Z. Formation of Stabilized Oblique Detonation Waves in a Combustor. *Combust. Flame* **2021**, *223*, 423–436. [CrossRef]
48. Zhang, Z.; Ma, K.; Zhang, W.; Han, X.; Liu, Y.; Jiang, Z. Numerical Investigation of a Mach 9 Oblique Detonation Engine with Fuel Pre-Injection. *Aerosp. Sci. Technol.* **2020**, *105*, 106054. [CrossRef]
49. Menter, F.R. Two-Equation Eddy-Viscosity Turbulence Models for Engineering Applications. *AIAA J.* **1994**, *32*, 1598–1605. [CrossRef]
50. McBride, B.J.; Zehe, M.J.; Gordon, S. *NASA Glenn Coefficients for Calculating Thermodynamic Properties of Individual Species*; National Aeronautics and Space Administration: Washington, DC, USA, 2002.
51. Wilson, G.J.; MacCormack, R.W. Modeling Supersonic Combustion Using a Fully Implicit Numerical Method. *AIAA J.* **1992**, *30*, 1008–1015. [CrossRef]
52. Wu, K. Investigation on the Flame Stabilization Modes and Chemical Mechanism Reduction in Supersonic Combustion. Ph.D. Thesis, University of Chinese Academy of Sciences, Beijing, China, 2018.
53. Choi, J.-Y.; Jeung, I.-S.; Yoon, Y. Computational Fluid Dynamics Algorithms for Unsteady Shock-Induced Combustion, Part 1: Validation. *AIAA J.* **2000**, *38*, 1179–1187. [CrossRef]
54. Teng, H.; Liu, S.; Zhang, Z. Unsteady Combustion Mode with a Super-High Frequency Induced by a Curved Shock. *Phys. Fluids* **2020**, *32*, 116101. [CrossRef]
55. Karl, S.; Hannemann, K.; Mack, A.; Steelant, J. CFD Analysis of the HyShot II Scramjet Experiments in the HEG Shock Tunnel. In Proceedings of the 15th AIAA International Space Planes and Hypersonic Systems and Technologies Conference, Dayton, OH, USA, 28 April–1 May 2008; American Institute of Aeronautics and Astronautics: Dayton, OH, USA, 2008.
56. Chapuis, M.; Fedina, E.; Fureby, C.; Hannemann, K.; Karl, S.; Martinez Schramm, J. A Computational Study of the HyShot II Combustor Performance. *Proc. Combust. Inst.* **2013**, *34*, 2101–2109. [CrossRef]
57. Chan, J.; Sislian, J.P.; Alexander, D. Numerically Simulated Comparative Performance of a Scramjet and Shcramjet at Mach 11. *J. Propuls. Power* **2010**, *26*, 1125–1134. [CrossRef]
58. Chakravarthy, S. A Unified-Grid Finite Volume Formulation for Computational Fluid Dynamics. *Int. J. Numer. Methods Fluids* **1999**, *31*, 309–323. [CrossRef]
59. Peroomian, O.; Chakravarthy, S.; Goldberg, U.; Peroomian, O.; Chakravarthy, S.; Goldberg, U. A "grid-Transparent" Methodology for CFD. In Proceedings of the 35th Aerospace Sciences Meeting and Exhibit, Reno, NV, USA, 6–10 January 1997; Aerospace Sciences Meetings; American Institute of Aeronautics and Astronautics: Reston, VA, USA, 1997.